# The $S_3$ State of the Oxygen-Evolving Complex in Photosystem II Is Converted to the $S_2Y_Z^\bullet$ State at Alkaline pH[†,‡]

Paulina Geijer,[§] Fatemeh Morvaridi, and Stenbjörn Styring*

*Biochemistry, Center for Chemistry and Chemical Engineering, Lund University, P.O. Box 124, S-221 00 Lund, Sweden*

*Received January 5, 2001; Revised Manuscript Received July 3, 2001*

ABSTRACT: Here we report an EPR signal that is induced by a pH jump to alkaline pH in the $S_3$ state of the oxygen-evolving complex in photosystem II. The $S_3$ state is first formed with two flashes at pH 6. Thereafter, the pH is changed in the dark prior to freezing of the sample. The EPR signal is 90−100 G wide and centered around $g = 2$. The signal is reversibly induced with a p$K = 8.5 \pm 0.3$ and is very stable with a decay half-time of 5−6 min. If the pH is changed in the dark from pH 8.6 to 6.0, the signal disappears although the $S_3$ state remains. We propose that the signal arises from the interaction between the Mn cluster and $Y_Z$, resulting in the spin-coupled $S_2Y_Z^\bullet$ signal. Our data suggest that the potential of the $Y_Z^\bullet/Y_Z$ redox couple is sensitive to the ambient pH in the $S_3$ state. The alkaline pH decreases the potential of the $Y_Z^\bullet/Y_Z$ couple so that $Y_Z$ can give back an electron to the $S_3$ state, thereby obtaining the $S_2Y_Z^\bullet$ EPR signal. The tyrosine oxidation also involves proton release from $Y_Z$, and the results support a mechanism where this proton is released to the bulk medium presumably via a close-lying base. Thus, the equilibrium is changed from $S_3Y_Z$ to $S_2Y_Z^\bullet$ by the alkaline pH. At normal pH (pH 5.5−7), this equilibrium is set strongly to the $S_3Y_Z$ state. The results are discussed in relation to the present models of water oxidation. Consequences for the relative redox potentials of $Y_Z^\bullet/Y_Z$ and $S_3/S_2$ at different pH values are discussed. We also compare the pH-induced $S_2Y_Z^\bullet$ signal with the $S_2Y_Z^\bullet$ signal from $Ca^{2+}$-depleted photosystem II.

Photosynthetic water oxidation to molecular oxygen is carried out by photosystem II (PSII)[1] in the thylakoid membrane of algae and higher plants. PSII is a large enzyme that is composed of at least 25 different polypeptides (*1, 2*). The inner core of PSII, the D1 and D2 proteins, has great structural and functional similarities to the photosynthetic reaction center of purple bacteria (*1, 3, 4*). The redox components involved in the oxidation of water are, however, unique to PSII.

The electrons from water are transferred to the quinone electron acceptors through redox cofactors coordinated by the D1/D2 heterodimer of PSII. Upon excitation by light, the primary electron donor, P680, reduces the primary pheophytin acceptor. To stabilize this charge-separated state, the electron is rapidly transferred to the first quinone acceptor ($Q_A$) and finally to the second plastoquinone acceptor in the $Q_B$ site (*2, 5, 6*). $P680^+$, the oxidized primary donor, is reduced by the redox-active tyrosine $Y_Z$ which, in its turn, is reduced by electrons from water bound to the oxygen-evolving complex (OEC). The OEC contains a cluster of four Mn ions and $Ca^{2+}$ and $Cl^-$ ions as cofactors (*2, 5*−*7*).

During water oxidation, OEC cycles through five different oxidation states, denoted $S_0$−$S_4$, where the subscript represents the number of stored oxidizing equivalents (*8*). $S_0$ is the most reduced state (*9*−*11*), and two of the manganese ions are generally thought to be present as Mn(II) and Mn(III). The valence of the other two manganese ions can be either Mn(III) or Mn(IV) (*8*−*13*). The $S_1$ state is the dark-stable state, and the $S_2$ and $S_3$ states are intermediates with high midpoint redox potentials (*14, 15*). The $S_4$ state is a transition state between the $S_3$ and $S_0$ states, where $S_3 \rightarrow S_4$ is a light-induced step and molecular oxygen is evolved during the spontaneous $S_4 \rightarrow S_0$ transition (*6, 7, 13, 16*).

The transition from $S_0$ to $S_1$ involves oxidation of manganese (*9*−*12, 17, 18*). It is thought that the $S_1$ to $S_2$ transition also involves oxidation of manganese, but it is less clear what is oxidized in OEC in the $S_2 \rightarrow S_3$ transition (*8, 12, 13, 17, 18*). Recent results on substrate water exchange (*19, 20*), and many other studies (*8, 21*−*24*), indicate that Mn is not oxidized in the $S_2 \rightarrow S_3$ transition. Instead, either a ligand to Mn, substrate water, or an oxo-bridge becomes oxidized. In contrast, other investigations point toward a Mn-

[†] This work was supported by the Knut and Alice Wallenberg Foundation, the Sven and Lily Lawski Foundation, DESS, The Swedish Energy Authority, and the Swedish Natural Science Research Council. P.G. and F.M. were recipients of grants from the Sven and Lily Lawski Foundation.

[‡] We dedicate this paper to the memory of Prof. Gerald T. Babcock, Michigan State University, East Lansing, MI, who inspired us in this work and participated in our discussions about the results.

* Corresponding author. Phone: +46 46 222 01 08; Fax: +46 46 222 45 34; E-mail: stenbjorn.styring@biokem.lu.se.

[§] Present address: Department of Biochemistry, 474 Medical Sciences Building, University of Alberta, Edmonton, Alberta T6G 2H7, Canada.

[1] Abbreviations: CAPS, 3-(cyclohexylamino)-1-propanesulfonic acid; Chl, chlorophyll; Cyt, cytochrome; DMSO, dimethyl sulfoxide; EDTA, ethylenediaminetetraacetic acid; EPR, electron paramagnetic resonance; Hepes, 4-(2-hydroxyethyl)piperazineethanesulfonic acid; Mes, 4-morpholineethanesulfonic acid; OEC, oxygen-evolving complex; PpBQ, phenyl-*p*-benzoquinone; PSII, photosystem II; $SII_{slow}$, the electron paramagnetic resonance signal from the neutral $Y_D^{ox}$ radical; $Y_Z$ and $Y_D$, the two redox-active tyrosine residues D1−161 and D2−161 in PSII.

10.1021/bi010040v CCC: $20.00 
Published on Web 08/14/2001

centered oxidation (*13*, *17*, *25*). Whether the formation of $S_3$ involves Mn oxidation or oxidation of another component is of central mechanistic importance, and mechanisms for oxygen evolution involving either alternative have been proposed (see *26* and references cited therein).

The OEC and $Y_Z$ interact closely during the oxidation of water. When $Y_Z$ is oxidized, the residue is deprotonated to form the neutral radical $Y_Z^{\bullet}$. The deprotonation involves His190 on the D1 protein, situated within hydrogen bonding distance from $Y_Z$ (*27*−*30*). Studies of light-induced electrochromic band-shifts indicate that the proton remains close to $Y_Z$, probably in the hydrogen bond to His190 (*31*−*35*). The interpretation of these data has been challenged, however, and others propose that the proton is expelled from PSII into the bulk solvent immediately after the oxidation of $Y_Z$ (*36*−*39*).

It is important to resolve the fate of the tyrosyl proton since it has consequences for how the reduction of $Y_Z^{\bullet}$ occurs. If the proton remains close to $Y_Z^{\bullet}$, the very oxidizing radical [+0.95−1.0 V at pH 6.5 (*15*, *40*)] is probably reduced by an electron from water mediated by the OEC concomitant with the return of the proton. In contrast, if the proton is expelled from PSII into the bulk solvent, the reduction of $Y_Z^{\bullet}$ is likely to involve hydrogen-atom transfer or proton-coupled electron transfer from the OEC (*38*, *39*). The latter mechanism is energetically and chemically favorable (*37*, *41*, *42*), but the available experimental evidence for the mechanism is still inconclusive. One possibility is that the different S-state transitions utilize different electron-transfer mechanisms from the OEC to $Y_Z^{\bullet}$.

There are many open questions about the OEC during the oxygen-evolving cycle. The least well understood intermediates are $S_3$ and $S_4$. One reason is the lack of spectroscopic probes from these states, and only recently EPR signals from the $S_3$ state were detected (*43*, *44*). Despite the lack of spectroscopic probes for the $S_3$ state in intact PSII, much information has been gained about the $S_2 \rightarrow S_3$ transition and the distance between $Y_Z$ and the Mn cluster from studies in partially inhibited PSII centers. After treatments that remove or modify the binding of the cofactors, $Ca^{2+}$ and $Cl^-$, the S-state cycle is perturbed, and the oxygen evolution is lost. The block in the S-cycle occurs between $S_2$ and $S_3$ and results in an EPR signal that arises from an oxidized organic radical in magnetic interaction with the Mn cluster (*45*−*47*). Since the discovery of the radical EPR signal in $Ca^{2+}$-depleted samples, analogous EPR signals have been detected also in samples inhibited with ammonia, fluoride, or acetate [reviewed in (*7*)]. The radical EPR signal is between 100 and 300 G wide (depending on the inhibitory treatment). There is now a general agreement that the OEC is present in the $S_2$ configuration and that the radical is $Y_Z^{\bullet}$ (*48*−*54*). The spin-coupled radical signal is therefore denoted the $S_2Y_Z^{\bullet}$ signal and is formed when the $Y_Z^{\bullet}$ radical is unable to oxidize the $S_2$ state in inhibited centers. Thus, the signal has until now only been observed in centers that never reached the real $S_3$ state.

Here we report the induction of the $S_2Y_Z^{\bullet}$ spin-coupled radical signal by increasing the pH in the dark in the $S_3$ state that was formed by two excitation flashes given at normal pH. We propose that the result of the increased pH value is a decreased reduction potential of $Y_Z^{\bullet}$, thereby shifting the equilibrium from $S_3Y_Z$ to $S_2Y_Z^{\bullet}$ in the dark. The results are discussed in light of the different models of hydrogen bonding of $Y_Z$ and compared with the results of the induction of the $S_2Y_Z^{\bullet}$ radical with other types of modifications.

Scheme 1: Description of the Experimental Procedures Used To Prepare EPR Samples To Test the Changes Induced by the pH-Jump (Top) and the Reversibility of the pH-Induced Changes (Bottom)

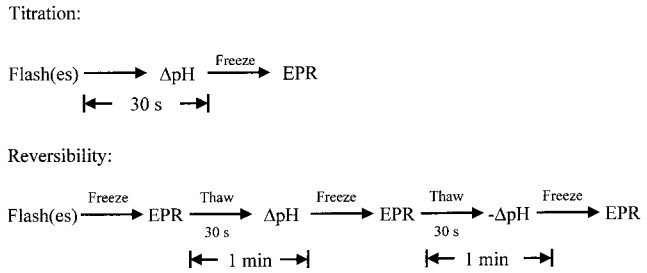


## MATERIALS AND METHODS

*PSII Preparation.* PSII-enriched membranes were prepared according to Pace et al. (*55*) from greenhouse-grown spinach cultivated on liquid culture medium. The preparations were stored at −80 °C at approximately 10 mg of Chl/mL. The oxygen evolution was 350−400 $\mu$mol of $O_2$·(mg of Chl)$^{-1}$·h$^{-1}$. All chlorophyll determinations were made in 80% ice-cold acetone/20% water according to Arnon (*56*).

*Flash Advancement to the $S_3$ State and pH Titration in the $S_3$ State.* To synchronize PSII in the $S_1$ state, the PSII-enriched membranes (about 4 mg of Chl/mL in flash experiments) were treated with a preflash and subsequent dark adaptation in a weakly buffering medium (0.5 mM Mes, pH 6.0) as described previously (*57*, *58*). The synchronized PSII population was given two saturating flashes to induce the $S_3$ state. The flashes (6 ns, 532 nm, and 350 mJ) were given at 5 Hz from a frequency-doubled Nd:YAG laser (Spectra Physics). The experimental flashes were given in the presence of 0.5 mM PpBQ (in DMSO) as exogenous electron acceptor. The two flashes and the subsequent 30 s mixing procedure (see below) resulted in 65−70% $S_3$ state. The fraction of each S state is determined from the flash-number-dependent oscillations of the $S_2$ and $S_0$ state multiline EPR signals over a flash sequence as described in references (*9*, *57*, *58*).

To study the effects of pH on the $S_3$ state, the pH was adjusted immediately after the excitation flashes (Scheme 1). pH was changed by adding buffer solutions in the pH range 4.0−11.0: DL-glutamic acid/KOH (pH 4.0−5.0), Mes/KOH (pH 5.0−7.0), Hepes/KOH (pH 7.0−8.0), glycylglycine/KOH (pH 8.0−9.75), or CAPS/KOH (pH 9.75−11). The final pH-buffer concentration was 14 mM. To allow thorough mixing, the buffers were added and mixed using a syringe with a spiral-shaped tip. The samples were frozen 30 s after the last flash. All procedures were carried out in dim green light. It should be emphasized that also the control samples were prepared exactly like this; i.e., a more concentrated buffer at pH 6 was added after the flashes.

*Reversibility Experiment.* The reversibility of the pH-induced modifications was investigated as described by Geijer et al. (*58*). Preflashed samples were given two flashes at pH 6.0 (0.5 mM Mes) and were rapidly frozen for EPR measurements (Scheme 1). After the first EPR measurement,

Table 1: Comparison between the $S_2Y_Z^\bullet$ Radical Signal Induced either with Alkaline pH (pH 8.6) or in $Ca^{2+}$-Depleted PSII Membranes

| treatment | $O_2$ evolution (%)[a] | signal width (G) | amplitude (au)[b] | % $S_2Y_Z^\bullet$ | lifetime[e] (s) |
|---|---|---|---|---|---|
| $Ca^{2+}$-depletion | 25 ($-Ca^{2+}$)<br>85 ($+Ca^{2+}$) | 110 | 1.0 | 75[c] | 15 |
| alkaline pH | nd | 90−100 | 0.45−0.50 | 50−55[d] | 300−360 |

[a] Oxygen evolution determined as described under Materials and Methods. The maximum $O_2$ evolution in untreated PSII membranes was 350−400 $\mu$mol of $O_2$·(mg of Chl)$^{-1}$·h$^{-1}$. nd: not determined. [b] The amplitude was estimated from the areas of those parts of the split signal that lie outside the peak of $Y_D$ (see Materials and Methods). [c] Percent of PSII centers forming the $S_2Y_Z^\bullet$ radical after $Ca^{2+}$-depletion (see text). [d] Percent of the $S_3$ state centers that gave rise to the $S_2Y_Z^\bullet$ signal. [e] Measured at 20 °C in the presence of 0.5 mM PpBQ. The lifetime of the $S_2Y_Z^\bullet$ radical in $Ca^{2+}$-depleted samples is taken from Andréasson et al. (*60*).

the samples were thawed for 30 s, and buffer at pH 9.0 (final concentration, 14 mM glycylglycine) was added (final pH = 8.6). The samples were incubated for 30 s and frozen for a second EPR measurement. The thawing and pH-buffer incubation were repeated once. This time the pH value of the sample was changed with a buffer at pH 6.0 (final concentration, 45 mM Mes) for the final EPR measurements (final pH = 6.2). The time was carefully monitored to allow control of the decay of the $S_2Y_Z^\bullet$ signal during the additions of the different pH buffers. After the EPR measurements, the samples were thawed, and the pH value, steady-state $O_2$ evolution at pH 6.0, and Chl concentration were determined. Parallel samples were made, where only the first pH adjustment buffer was added to allow determination of the pH value obtained after the first pH addition.

*$Ca^{2+}$-Depletion of PSII and Induction of the $S_2Y_Z^\bullet$ Signal.* $Ca^{2+}$ was removed from PSII by treatment at low pH in the presence of citrate as in (*47, 59*). The $Ca^{2+}$-depleted samples exhibited about 25% of the normal steady-state $O_2$ evolution in the absence of $Ca^{2+}$ (Table 1). In the presence of $Ca^{2+}$, the oxygen evolution increased to 80−85% of the control oxygen evolution. This is normal for a preparation of $Ca^{2+}$-depleted PSII (*47, 59, 60*), and this level of recovery of the oxygen evolution indicates that almost all centers are functional in the sense that they possess a nondestroyed OEC. Often, only 80−85% of the initial activity is regained by $Ca^{2+}$ re-addition due to modifications on both the donor and the acceptor side of PSII (*60*). The lowered maximal oxygen evolution after $Ca^{2+}$ addition is therefore probably not due to loss of the Mn cluster. We conclude that in our preparation about 25% of the OEC are fully functional and have not lost their $Ca^{2+}$. The remaining 75% of the centers have lost $Ca^{2+}$ and give rise to the $S_2Y_Z^\bullet$ radical signal.

Maximal induction of the $S_2Y_Z^\bullet$ radical in the $Ca^{2+}$-depleted PSII was achieved by illumination at 0 °C in the presence of 0.5 mM PpBQ. The samples were illuminated 30 s using heat-filtered white light from an 800 W lamp. This protocol is known to induce almost stoichiometric amounts of the $S_2Y_Z^\bullet$ signal from PSII centers that lack $Ca^{2+}$ (*60, 61*). Light saturation was also confirmed by the complete disappearance of the stable multiline signal from the modified $S_2$ state in the $Ca^{2+}$-depleted PSII upon formation of the $S_2Y_Z^\bullet$ radical (*45, 62*). Thus, in our $Ca^{2+}$-depleted PSII samples, the maximal $S_2Y_Z^\bullet$ signal arose from 75% of the PSII centers (Table 1). We used this signal to quantify our pH-induced $S_2Y_Z^\bullet$ radical that has a very similar spectral shape. For the quantification, we directly compared the area of the parts of the split signal that lies outside the spectrum from $Y_D$ (compare Figure 1B), by assuming a similar Gaussian line shape in each part of the split signal. The splitting of the signal in $Ca^{2+}$-depleted PSII is 10−20% wider than our pH-induced signal (Table 1).

*EPR and Data Analysis.* Low-temperature continuous-wave EPR measurements were performed with a Bruker ESP500e spectrometer using a SuperX ER049X microwave bridge. The system was fitted with a liquid helium cryostat and temperature controller from Oxford Instruments Ltd. Spectrometer settings are given in the figure legends. The measurements were performed either with a Bruker 4102 standard cavity or with a Bruker ER4122SHQ cavity, which provides about 8 times better signal-to-noise ratio.

The intensity of the $S_2Y_Z^\bullet$ EPR signal in the pH titration was estimated from the peak to trough amplitudes at the field positions indicated with bars in Figure 1B. The intensity was normalized to the Chl concentration to compensate for differences in sample concentration.

The titration curve of the $S_2Y_Z^\bullet$ radical was fitted from pH 4.5−9.4 with a single p$K$ according to eq 1:

$$y = c/(1 + 10^{(pK-pH)}) \quad (1)$$

Here, $y$ is the measured EPR signal amplitude, p$K$ is the apparent p$K$ of the induction of the $S_2Y_Z^\bullet$ signal, and $c$ is the proportionality constant.

*Steady-State $O_2$ Evolution.* Steady-state $O_2$ evolution was measured on two different kinds of samples: the EPR samples and samples incubated 30 s at pH 8.6 and room temperature without the freezing/thawing cycle. The latter samples were used to estimate the destruction of PSII centers during the decay experiment. Steady-state $O_2$ evolution was measured with a Clark-type electrode at 20 °C in a medium containing 20 mM Mes/KOH, 10 mM $MgCl_2$, 10 mM NaCl, 5 mM $CaCl_2$, and 400 mM sucrose at pH 6.0, with 0.5 mM PpBQ (in DMSO) added as the external acceptor. Illumination was supplied from a saturating white light-source. The EPR samples were thawed for 30 s, and an aliquot of 20 $\mu$g of Chl for each EPR sample was added to 1 mL of medium. The $O_2$ evolution was always measured at pH 6.0, irrespective of the pH value of the EPR sample.

## RESULTS

*Induction of an EPR Signal in the $S_3$ State at Elevated pH.* When dark-adapted PSII centers are given saturating laser flashes, the OEC cycles through the different S states, that can be studied by EPR spectroscopy. After one flash at pH 6−7, the $S_2$ state is formed, resulting in the $S_2$ multiline signal (Figure 1A, a) (*63*). After two flashes, the $S_3$ state is formed, and the $S_2$ multiline signal becomes much smaller (Figure 1B, b). There is 20−25% $S_2$ multiline signal remaining after two flashes. This is due to the misses; i.e.,

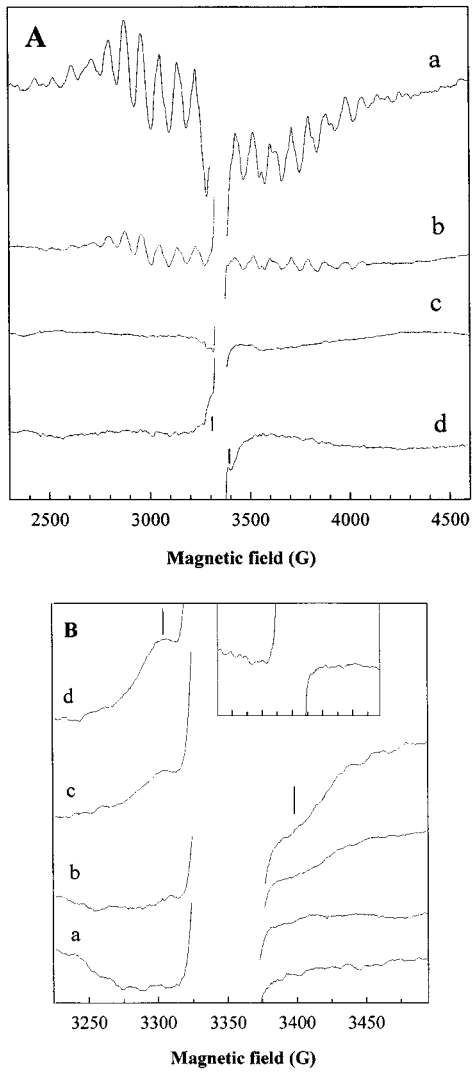


FIGURE 1: Induction of a split radical EPR signal at elevated pH in the $S_3$ state. EPR spectra at pH 6.0 and 8.6 of PSII-enriched samples given 1 and 2 flashes. (A) Spectra of 1- and 2-flash samples from pH-treated samples. The samples were treated as described for the pH titration experiment. Spectrum (a), 1 flash + pH 6.0, (b) 2 flashes + pH 6.1, (c) 1 flash + pH 8.8, and (d) 2 flashes + pH 8.9. The bars indicate the field positions for the maximum and minimum amplitudes of the pH-induced spectrum in the 2-flash sample. EPR settings: microwave power 16 mW; microwave frequency 9.40 GHz; temperature 7 K; modulation frequency 100 kHz; modulation amplitude 14 G. The spectra are normalized for differences in chlorophyll concentration. The large $SII_{slow}$ has been omitted in all the spectra for clarity. (B) EPR spectra of 2-flash samples at four different pH values: (a) pH 6.1, (b) pH 7.5, (c) pH 8.4, and (d) pH 8.9. The spectra are normalized to the chlorophyll concentration of the samples. The large $SII_{slow}$ has been omitted in all the spectra for clarity. EPR settings: microwave power 25.4 mW; microwave frequency 9.40 GHz; temperature 7 K; modulation frequency 100 kHz; modulation amplitude 5 G. The inset shows the radical region of a spectrum from a sample given 1 flash at pH 6 after which the pH was raised to pH 8.6. The inset is shown to clarify that the $S_2Y_Z^\bullet$ radical is absent after one flash in a sample at high pH. The magnetic field scale is the same as in (B).

the OEC does not turn over as a consequence of a flash. In our flash protocol, the misses amount to about 13% on each flash (*9, 58*). There are no EPR signals observable from the centers that are in the $S_3$ state after the two flashes at pH 6−7 (70−75%).

When the pH was raised by the addition of alkaline buffer in the dark, after the two flashes, the EPR spectrum changed dramatically. Two effects were observed: First, the remaining $S_2$ multiline signal disappeared as described in ref (*58*) (Figure 1A, c). Second, the appearance of an EPR signal centered around $g = 2$ was observed (Figure 1A, d). The signal is visible as a shoulder and a trough on the low- and high-field sides, respectively, of the narrower radical signal from $Y_D^\bullet$ and is indicated by bars in the spectrum (Figure 1A, d). The signal is better observed in the spectra recorded with higher resolution in Figure 1B.

The EPR signal observed after two flashes and alkaline pH treatment is about 90−100 G wide (Figure 1B). The general shape of the signal is similar to the EPR signal first discovered in $Ca^{2+}$-depleted PSII samples after illumination (*45*−*47, 64*). This signal is known to originate from the magnetic interaction between $Y_Z^\bullet$ and the $S_2$ state of the OEC (*48*−*54, 65*). Therefore, we tentatively also assign the pH-induced signal to the $S_2Y_Z^\bullet$ state. The signal presented here is formed after two flashes by the addition of alkaline buffer in the dark. The signal is formed neither in the flash-induced $S_2$ state when exposed to alkaline pH (cf. Figure 1A, c, and inset in Figure 1B) nor in the $S_0$ state [see Geijer et al. (*58*)]. Therefore, we assign the signal to centers poised in the $S_3$ state prior to the addition of alkaline pH.

*Quantification of the EPR Signal.* A crucial issue is whether the pH-induced, split EPR signal represents a large fraction of the PSII centers that were in the $S_3$ state. The $S_2Y_Z^\bullet$ signal has proved difficult to quantify with precision. However, it has become clear that the $S_2Y_Z^\bullet$ signal is formed quantitatively when $Ca^{2+}$-depleted PSII centers are illuminated at 0 °C in the presence of an electron acceptor (*61, 66*). We have used this to attempt a rough quantification of the pH-induced $S_2Y_Z^\bullet$ signal (Table 1).

The amplitude of the pH-induced radical signal is maximal around pH 8.5−9.0 (see below). The signal originates from the 65−70% of the PSII centers that were in the $S_3$ state after the two flashes and the 30 s incubation for addition and mixing. (Note that the 30 s incubation resulted in ≈10% decay of $S_3$. Therefore, only 65−70% of PSII was in the $S_3$ state in this experiment.) The remaining PSII centers do not give rise to the $S_2Y_Z^\bullet$ signal.

In our preparation of $Ca^{2+}$-depleted PSII, the $S_2Y_Z^\bullet$ signal was induced in 75% of the PSII centers (see Materials and Methods). We compared the size of this signal with the pH-induced signal at pH 8.6 by normalization and correction for the centers available to form the split signal in each case (65−70% in the $S_3$ state and 75% in the $Ca^{2+}$-depleted sample). This comparison revealed that the radical signal observed at pH 8.6 originated from 50 to 55% of the PSII centers that were in the $S_3$ state. This quantification is approximate, but it is clear that the $S_2Y_Z^\bullet$ signal could be formed in a large fraction of the centers that were in the $S_3$ state prior to the pH change. It is possible that our $Ca^{2+}$-depleted PSII contained a fraction of Mn-depleted centers (<20%, see Materials and Methods). This would lower the fraction of PSII giving rise to the split signal in this material and consequently also lower the fraction of centers giving rise to the split EPR signal in the $S_3$ state at high pH. However, also in this case, the pH-induced signal at pH 8.6 would constitute >40−45% of the PSII centers that were in the $S_3$ state.

*pK of the Induction of the $S_2Y_Z^\bullet$ Radical EPR Signal.* The pH-induced EPR signal from $S_2Y_Z^\bullet$ formed from the $S_3$ state

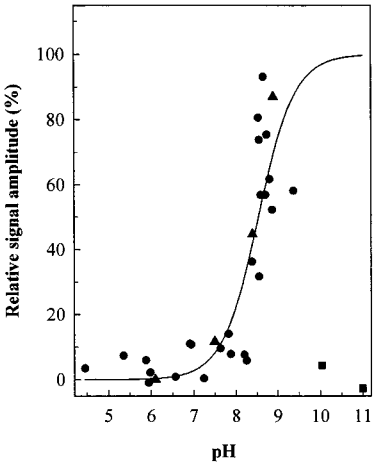


FIGURE 2: Titration of the pH-induced EPR signal in the $S_3$ state. The data points reflect the peak to trough amplitude of the $S_2Y_Z^\bullet$ signal as shown in Figure 1B. Points indicated with triangles represent the spectra shown in Figure 1B. The intensity of the signal is normalized to differences in chlorophyll concentration. Above pH 9, the sample starts to be negatively affected by the alkaline pH (see text), and the amplitude of the EPR signal above pH 9.5 is very low due to the disintegration of the Mn cluster and PSII (squares). The fitting of the data from pH 4.4 to 9.4 was made according to eq 1. The maximum level of the signal was estimated by comparison with the $S_2Y_Z^\bullet$ signal from a $Ca^{2+}$-depleted sample (see text and Table 1). The apparent p*K* for the increase of the signal was determined to be 8.5 ± 0.3.

is shown in detail at different pH values in Figure 1B. Spectra a−d were recorded at pH 6.1, 7.5, 8.4, and 8.9, respectively. At pH 6.1 no $S_2Y_Z^\bullet$ signal is observable after two flashes, at pH 7.5 there is a very small signal, at pH 8.4 the signal is clearly visible, and at pH 8.9 the signal is even larger.

In Figure 2, the pH titration of the induction of the $S_2Y_Z^\bullet$ signal between pH 4.5 and 10 is shown. Between pH 4.5 and 7, no signal is detected. In the pH region 8−9, there is a rapid increase of the signal amplitude to its maximum amplitude. In samples at pH 9.4 or more, the signal becomes smaller again. Above pH 9.4, we observe an irreversible loss of the oxygen evolution in a large fraction of centers (see below), and Mn release is also observed in the EPR spectra (not shown). These observations indicate that at extreme pH values (above pH 9.4) the OEC is quickly destroyed irreversibly by the pH. This is not unexpected, and it is known that the OEC is sensitive to incubation at alkaline pH values (in our case for 30 s). It is therefore concluded that the decrease in the $S_2Y_Z^\bullet$ signal amplitude at pH >9.4 is not related to the same process that lead to induction of the signal between pH 7.5 and 9.

We have estimated that the pH-induced $S_2Y_Z^\bullet$ signal at pH 8.6 corresponds to about 55% of the centers in the $S_3$ state. This makes it possible to estimate the p*K* for the induction of the signal. In Figure 2, the pH-dependent change of the $S_2Y_Z^\bullet$ signal amplitude is fitted with an equation with a single p*K* (see Materials and Methods). The p*K* determined for the induction of the $S_2Y_Z^\bullet$ signal from the $S_3$ state is 8.5 ± 0.3. This p*K* is higher than the p*K* values determined for the decrease of the amplitudes in the alkaline region of the $S_0$ and $S_2$ multiline signals (*58*). In the study of the $S_0$ and $S_2$ multilines, p*K* values of 8.0 and 7.6, respectively, were observed.

*Lifetime of the pH-Induced $S_2Y_Z^\bullet$ Signal.* The lifetime of the EPR signal was probed by recording the EPR spectra in

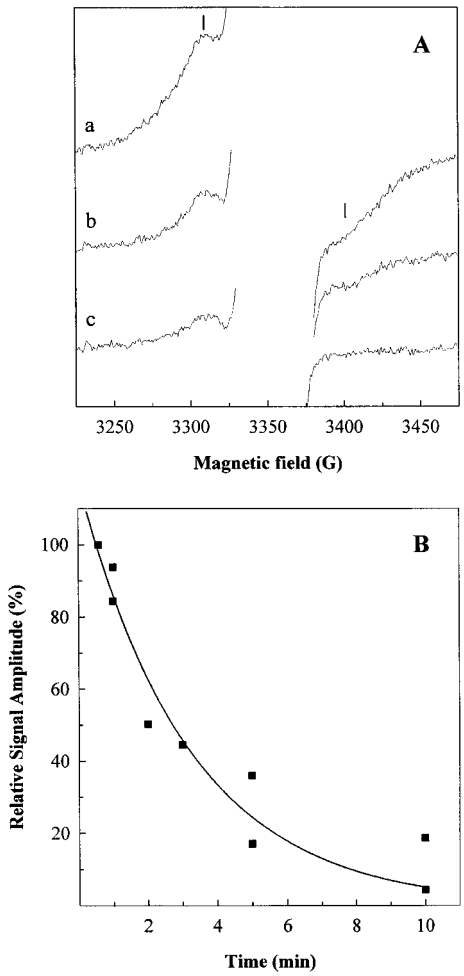


FIGURE 3: Decay at 20 °C of the radical signal at pH 8.6. (A) EPR samples were prepared as for the pH titration experiment but were frozen at different times after the pH change in the $S_3$ state. The pH of the EPR samples was 8.6 ± 0.1. The EPR spectra represent the signal in samples frozen at different times: (a) frozen 35 s after the flashes, (b) 3 min after the flashes, (c) 10 min after the flashes. The bars indicate the signal width of the $S_2Y_Z^\bullet$ radical. EPR settings as in Figure 1B. Signal $II_{slow}$ has been omitted for clarity. (B) Decay of the radical at room temperature. The amplitudes are estimated as the peak to trough amplitudes of the EPR spectra in (A). The time where half of the $S_3$ signal had decayed was estimated to be 2.2 min (the curve in the figure). The observed decay reflects two events: the decay of the $S_3$ state and the damage of the Mn cluster (see text).

samples frozen at different times after the flashes and pH change to pH 8.6 ± 0.1. The decay at room temperature of the signal amplitude is shown in Figure 3. The decay of the amplitude was fitted with a 2.2 min half-time at pH 8.6. This is not, however, the real decay of the $S_2Y_Z^\bullet$ radical. At high pH, the OEC is sensitive and becomes irreversibly damaged. This is the case at pH 8.6, and during the 60 s incubation after the pH increase, about 30% of the oxygen-evolving capacity was lost (measured at pH 6.0) (Figure 4C). During the much longer incubation in the decay experiment described in Figure 3, the damage is even more severe. The oxygen evolution is irreversibly lost with a half-time of about 3.5−4 min during the incubation at pH 8.6 (not shown).

Thus, the decay of the signal amplitude described in Figure 3 represents a combination of the actual decay of the pH-induced $S_2Y_Z^\bullet$ signal and the destruction of the OEC (probed with $O_2$ evolution measurements). From the measured decay

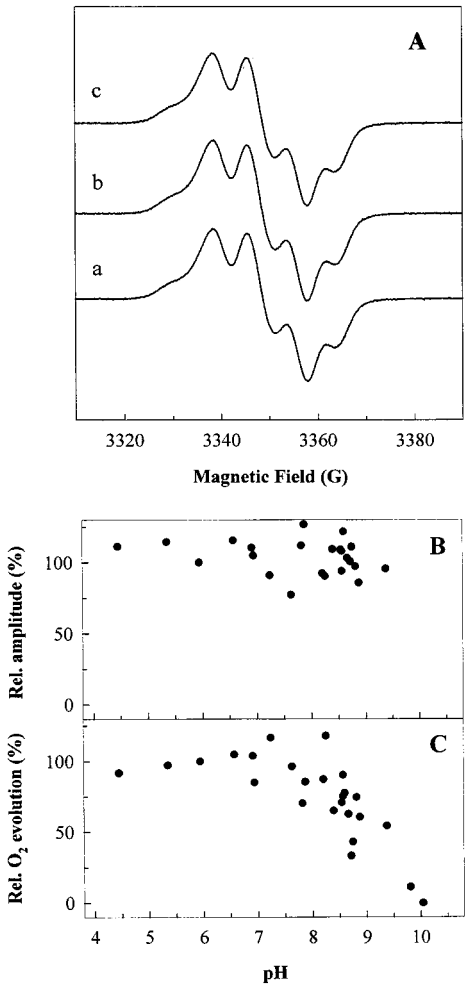


FIGURE 4: Effect of pH treatment on $SII_{slow}$ and $O_2$ evolution in the samples given two flashes. (A) EPR spectra of $SII_{slow}$ in the samples from the titration curve at different pH values: (a) pH 6.1, (b) pH 8.2, and (c) pH 8.6. The spectra are normalized to differences in the chlorophyll concentration. EPR settings: microwave power 1.01 $\mu$W; microwave frequency 9.47 GHz; temperature 15 K; modulation frequency 100 kHz; modulation amplitude 3.2 G. (B) pH titration of the amplitude of $SII_{slow}$. The signal amplitude is measured as the height of the low-field peak and is normalized to the chlorophyll concentration and the size of $SII_{slow}$ at pH 5.9. (C) Steady-state $O_2$ evolution measured at pH 6 of the EPR samples from Figure 1B. The samples were thawed for 30 s before an aliquot was added to the measuring medium. The total incubation time from flash to measurement of oxygen evolution was 60 s. The graph shows the normalized $O_2$ evolution. The samples are normalized to the remaining $O_2$ evolution in the pH 5.9 sample. The $O_2$ evolution in the pH 5.9 samples was 80% of the $O_2$ evolution in the freshly prepared PSII-enriched membranes.

of the signal (Figure 3) and from the observed damage of the OEC (3.5−4 min half-time, not shown), we can estimate that the real decay of the $S_2Y_Z^\bullet$ signal occurs with a half-time of 5−6 min at pH 8.6 and room temperature (Table 1). Thus, the signal decays much slower than the $S_2Y_Z^\bullet$ signal in $Ca^{2+}$-depleted or acetate-inhibited PSII which decays in 10−30 s dependent on temperature at pH 6.5 (*49*, *50*, *60*, *65*, *67*).

*$SII_{slow}$ and Steady-State Oxygen Evolution.* To determine the integrity of PSII, we followed how the pH affected $SII_{slow}$ (from $Y_D^\bullet$) and the steady-state $O_2$ evolution measured at pH 6. The EPR signal from $Y_Z^\bullet$ has a very similar shape to that of $SII_{slow}$. It is therefore important to follow the behavior of $SII_{slow}$. If an increase in $SII_{slow}$ was observed at any pH, this could indicate that a fraction of uncoupled $Y_Z^\bullet$ was produced. Figure 4A shows $SII_{slow}$ at pH 6.1, 8.2, and 8.6, and it is clear that the amplitude and spectral shape did not change substantially over this pH interval during the 30 s incubation. This is also shown in Figure 4B where the amplitude of $SII_{slow}$ is compared between pH 4.5 and 9.4. We conclude that we do not induce the uncoupled $Y_Z^\bullet$ radical in this pH interval.

The remaining $O_2$ evolution in our EPR samples exposed to different pH values was also measured at pH 6. In this and our previous study (*58*), the samples were treated with the pH buffers in the dark, but the $O_2$ evolution was measured at pH 6.0 [see Materials and Methods and (*58*)]. Samples treated with pH buffers in the range 4.5−7 display only minor variations in the steady-state $O_2$ evolution at pH 6 (Figure 4C), indicating that the experimental protocol does not damage any PSII centers in this pH interval. In samples exposed to pH >7−7.5, the $O_2$-evolving activity starts to decrease, indicating that the alkaline pH has an effect on the integrity of the Mn cluster (Figure 4C). At pH 8.6, about 30% of the $O_2$ evolution is lost. The decrease is caused by destruction of the Mn cluster partly due to the high pH values and partly due to thawing of the samples before the measurements.

*Reversibility of the Formation of the pH-Induced $S_2Y_Z^\bullet$ Signal.* At pH 8.6, the $S_2Y_Z^\bullet$ EPR signal corresponds to about 55% of the centers in the $S_3$ state (Figures 1B and 2). At this pH, $SII_{slow}$ was not significantly changed, and about 70% of the oxygen-evolving capacity remained (Figure 4B,C). This shows that the Mn cluster was not damaged in the large majority of the PSII centers by the pH change and the short incubation at pH 8.6.

This allowed us to test the reversibility of the formation of the $S_2Y_Z^\bullet$ EPR signal. The reversibility experiment was carried out as described in Scheme 1. In samples frozen at pH 6 immediately after the flashes, we could not observe any $S_2Y_Z^\bullet$ radical signal from the ≈75% of PSII centers that were in $S_3$ (Figure 5A,B, a). A small $S_2$ multiline signal was observed (Figure 5B, a) from approximately 20% of the PSII centers that were in the $S_2$ state due to misses in the flash excitation (see above). When the samples were thawed and the pH was changed to pH 8.6, a large $S_2Y_Z^\bullet$ radical signal was induced (Figure 5A,B, b). The signal size indicates that about 60−65% of the PSII centers remained in the $S_3$ state after thawing and incubation with the alkaline buffer. No $S_2$ multiline signal was observed (Figure 5B, b) at the high pH (*58*).

The sample was thawed again, and the pH was changed back to pH 6.2 (Figure 5A and B, c). This resulted in the disappearance of the 100 G wide $S_2Y_Z^\bullet$ signal. At the same time, a small $S_2$ state multiline signal representing about 7% of PSII appeared (Figure 5B, c). The fraction of centers in the $S_1$ state was estimated with an illumination at 200 K (which brings $S_1$ centers to the $S_2$ state), and it was found that about 20% of the PSII centers were in the $S_1$ state (not shown). The complex experimental protocol also led to the destruction of a fraction of the Mn clusters, and we estimate that the fraction of non-oxygen-evolving centers was about 35% after the pH changes and repeated freezing and thawing (not shown). Thus, we can account for 60−65% of the centers being either in the $S_1$ or in the $S_2$ states or being damaged. The remaining 35−40% of the PSII centers should

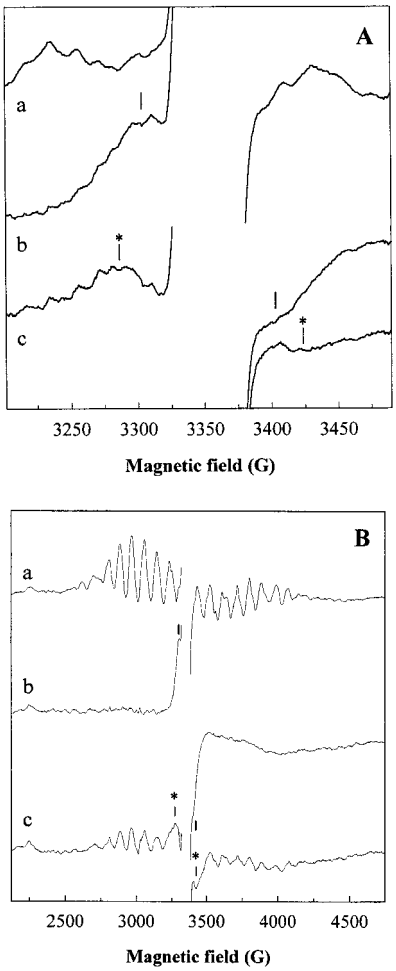


FIGURE 5: Formation of the $S_2Y_Z^\bullet$ signal from the $S_3$ state at alkaline pH is reversible. The experimental protocol is described in Scheme 1. (A) High-resolution spectra showing the region around $g = 2$ to allow observation of the $S_2Y_Z^\bullet$ signal. (a) A sample given 2 flashes at pH 6 and immediately frozen after the last flash. (b) The sample from (a) thawed and incubated at alkaline pH (final pH 8.6). (c) The sample in (b) thawed a second time with the pH changed back to 6.2. EPR settings as in Figure 1B. (B) EPR spectra recorded over a wider spectral region for the same samples as in (A) to allow simultaneous observation of the $S_2Y_Z^\bullet$ signal (partially resolved) and the $S_2$ multiline signal. EPR settings as in Figure 1A. The bars in (b) indicate the $S_2Y_Z^\bullet$ radical. The asterisks in (c) indicate the features of the broader EPR signal appearing after the pH had been reversed from 8.6 to 6.2. The spectra are normalized to differences in concentration using the amplitude of $SII_{slow}$. Signal $II_{slow}$ has been omitted for clarity.

be in the $S_3$ state. This is a large fraction of $S_3$ state centers, and since we observe no $S_2Y_Z^\bullet$ signal (Figure 5A, c), we conclude that the induction of the $S_2Y_Z^\bullet$ signal at alkaline pH involves a reversible change in the OEC in the $S_3$ state.

It is interesting that we observe another EPR signal in the samples after the return to pH 6.2. The $S_2Y_Z^\bullet$ radical with a spectral width of 90−100 G has disappeared, but a small, slightly broader feature appeared instead (Figure 5A,B, c, indicated with asterisks). This spectrum has some resemblance to the $S_2Y_Z^\bullet$ signal in acetate-inhibited samples (*51, 52, 54, 68, 69*). Presently we cannot ascertain whether this signal in Figure 5A and 5B, c, arises from a perturbed $S_3$ state or if it originates from damaged PSII or PSII in another S state where the perturbation is induced by the complex experimental protocol. We did not observe a similar signal when identical reversibility experiments were carried out in

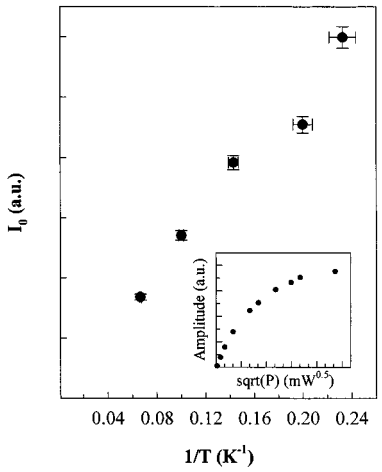


FIGURE 6: Temperature dependence of the high-pH-induced $S_2Y_Z^\bullet$ signal. Curie plot of the temperature dependence of the $S_3$ signal. The initial slope was determined as the first three points of the power saturation curve to make the data obtained at the different temperatures comparable. Inset: microwave power saturation curve at 7 K plotted with the signal intensity as a function of the square root of power. The scale of the *x*-axis in the inset ranges from 0 to 16 with major ticks every third integer (3, 6, 9, etc.). The EPR settings for the measurements are as in Figure 1B, except for the microwave power. The error in the temperature measurement was ±0.2 K, and the error in $I_0$ (determined from plots similar to that in the inset) was ±3%.

the $S_0$ or $S_2$ states (*58*). Thus, it is possible that the reaction is not fully reversible as the, so far unassigned, spectral species might originate from PSII centers that were in $S_3$ when they were exposed to the elevated pH.

*Microwave Power Saturation and Temperature Dependence of the pH-Induced $S_2Y_Z^\bullet$ Signal.* To further characterize the $S_2Y_Z^\bullet$ signal, we studied the microwave power and temperature dependence of the $S_2Y_Z^\bullet$ signal amplitude. The radical induced at alkaline pH is very difficult to saturate. The inset in Figure 6 shows the $S_2Y_Z^\bullet$ radical intensity as a function of the square root of the microwave power at 7 K. The $P_{1/2}$ determined at 7 K was 35 mW.

At nonsaturating microwave powers, the signal intensity increases linearly ($I_0$) with the square root of the microwave power. In Figure 6, we show the initial slope ($I_0$) of the $S_2Y_Z^\bullet$ signal amplitude at five different temperatures plotted as a function of $1/T$. The initial slope depends linearly on $1/T$ and extrapolates to the origin at high temperatures. This indicates that the $S_2Y_Z^\bullet$ radical arises from an isolated ground-state signal. The radical induced with the pH treatment is a very fast relaxer and shows higher $P_{1/2}$ values than the $S_2Y_Z^\bullet$ signal induced by $Ca^{2+}$-depletion or acetate treatment (*45, 69, 70*).

## DISCUSSION

Our results show that an increase of the pH to more alkaline pH values in the dark, in the $S_3$ state, leads to the formation of a split radical EPR signal. The signal is formed only from the $S_3$ state, and neither the $S_0$, $S_1$, nor $S_2$ states give rise to a similar signal.

The observed EPR signal is similar in width and temperature dependence to an EPR signal first detected more than 10 years ago in $Ca^{2+}$-depleted PSII (*45*−*47, 71, 72*) and also in $Cl^-$-depleted PSII (*67, 73*). In $Ca^{2+}$-depleted PSII, the signal was assigned to an organic radical species, magneti-

cally coupled to the Mn cluster in the $S_2$ state (*45*). At first, the radical species was proposed to be a histidine radical (*45, 71*), but the radical has now been identified as $Y_Z^\bullet$ (*48*−*50, 52, 54, 74*), and the signal is denoted the $S_2Y_Z^\bullet$ EPR signal. The signal from the $S_3$ state at alkaline pH cannot be unambiguously assigned at present. The similar line shape and fast relaxation properties are strongly suggestive that it originates from the same species as in $Ca^{2+}$- and $Cl^-$-depleted systems. Therefore, we assign our EPR signal to the $S_2Y_Z^\bullet$ state.

The pH-induced $S_2Y_Z^\bullet$ signal differs in some aspects from the previously presented $S_2Y_Z^\bullet$ signals. First, the pH-induced signal is formed in a different way. The $S_3$ state is induced by two flashes given at pH 6 to intact, oxygen-evolving PSII. The pH was changed in the dark after the flashes to induce the signal. Thus, the induction of the signal involves no illumination of PSII compared to the signals induced by $Ca^{2+}$- and $Cl^-$-depletion. The $S_2Y_Z^\bullet$ signal has not been induced in darkness before.

The pH-induced signal is also very stable. In oxygen-evolving PSII, $Y_Z^\bullet$ is stable for tens to hundreds of microseconds ($S_0$, $S_1$, and $S_2$) to about 1 ms ($S_3$) (*5, 16*). $Y_Z^\bullet$ in the $S_2Y_Z^\bullet$ signal in $Ca^{2+}$-depleted (*60*) or acetate-inhibited PSII (*49, 50*) is more stable and has a half-time for the decay of 5−15 s at pH 6.0−6.5 at room temperature. The pH-induced $S_2Y_Z^\bullet$ radical is even more stable, and the half-time was estimated to 5−6 min at pH 8.6. The increased stability of the $S_2Y_Z^\bullet$ signal at elevated pH values is an interesting property that probably reflects the reduction pathway for $Y_Z^\bullet$. This involves both reduction and protonation of the oxidized tyrosine. At high pH, there are fewer protons available, which results in slow reduction of the tyrosine radical.

We see two possibilities that can account for the formation of the $S_2Y_Z^\bullet$ signal at high pH. The first possibility is that the $S_2Y_Z^\bullet$ state represents the $S_3$ state. In this case, the effect of the alkaline pH is to alter the magnetic coupling between the Mn cluster and $Y_Z^\bullet$, making the $S_2Y_Z^\bullet$ signal observable. The possibility that $S_3$ involved an oxidized radical was proposed several years ago (*21, 45, 71*). However, the available kinetic data on $Y_Z^\bullet$ reduction indicate that $Y_Z^\bullet$ is reduced immediately upon the formation of $S_3$ (*75*−*77*). Therefore, it is improbable that $S_2Y_Z^\bullet$ dominates in the $S_3$ state.

The second possibility, which we find more attractive, is that the redox potential of the $Y_Z^\bullet/Y_Z$ couple is lowered by the alkaline pH. The potential of the free tyrosine radical is 970 mV at pH 5.0, and it decreases at 59 mV per pH unit as the pH is increased (*78*). The potential of $Y_Z^\bullet/Y_Z$ is quite similar to that of the free tyrosine radical and is about 970 mV at pH 6.0 [Figure 7; (*15*)]. If the increased pH in the bulk solvent indeed can affect the potential of $Y_Z^\bullet/Y_Z$, a pH increase from 6.0 to 8.5 would decrease the redox potential of $Y_Z^\bullet/Y_Z$ by about 150 mV, making the couple ≈820 mV at pH 8.5 (Figures 7 and 8). From our data, we know that the potentials of $S_3/S_2$ and $Y_Z^\bullet/Y_Z$ should be equal at pH 8.5, the p*K* of $S_2Y_Z^\bullet$ signal induction. The $S_3/S_2$ redox couple is thought to be only 40 mV less oxidizing than $Y_Z^\bullet/Y_Z$ at pH 6 [Figure 7; (*15, 79*)]. However, it is not certain that this is the case, and the potential of $S_3/S_2$ must be either pH-dependent to obtain a p*K* of 8.5 for induction of the $S_2Y_Z^\bullet$ signal (Figure 8, dashed line) or less oxidizing than previously estimated (Figure 8, dotted line).

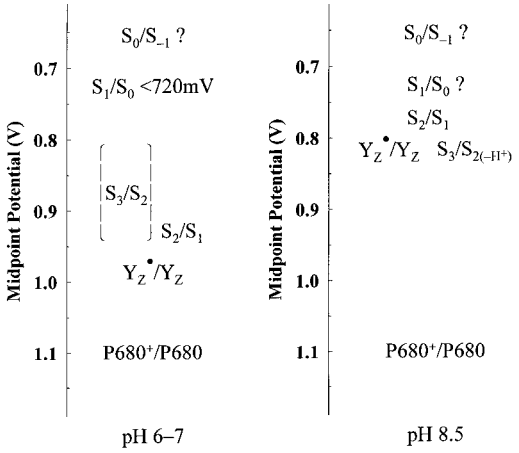


FIGURE 7: Diagram showing the relative redox potentials in the oxygen-evolving complex at two different pH values. The numbers at pH 6−7 are taken from Vass and Styring (*15*) and references cited therein. When the pH is increased in the bulk solvent, the $Y_Z^\bullet/Y_Z$ couple is proposed to become less oxidizing. The redox potential of the $S_3/S_2$ couple is proposed to be lower than previously thought and independent of pH while the potential of the $S_2/S_1$ couple is proposed to be pH-dependent. The situation is less clear for the $S_1/S_0$ and $S_0/S_{-1}$ redox couples. See text for discussion.

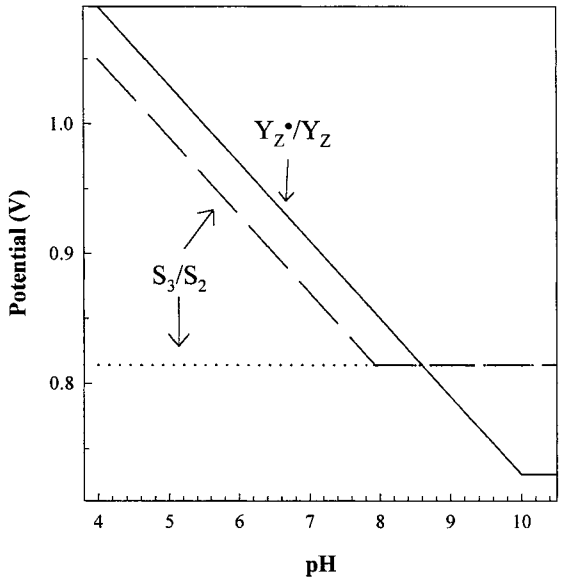


FIGURE 8: Hypothetical presentation on how the relative potentials of $Y_Z^\bullet/Y_Z$ and $S_3/S_2$ are affected by pH. Two alternatives are shown for the $S_3/S_2$ couple: either the potential is 40 mV lower than that of $Y_Z^\bullet/Y_Z$ (*81*) at pH 6 and pH-dependent, or the potential is lower at pH 6 and pH-independent (see text). The solid line represents $Y_Z^\bullet/Y_Z$, the dashed line $S_3/S_2$ (pH-dependent), and the dotted line $S_3/S_2$ (pH-independent). The $S_3/S_2$ and $Y_Z^\bullet/Y_Z$ potential curves have to cross at pH 8.5, the p*K* value determined for the induction of the $S_2Y_Z^\bullet$ signal. The relative redox potentials at pH 6 for $Y_Z^\bullet/Y_Z$ and $S_3/S_2$ were estimated by Vos (*79*) and Vass and Styring (*15*). The decrease of the potential with ≈60 mV per pH unit is characteristic of a one-electron/one-proton reaction. Thorp et al. (*89*) and Baldwin et al. (*90*) determined pH-dependent redox potentials for Mn compounds and Tommos et al. (*78*) for tyrosine in solution.

In the first case (Figure 8, dashed line), the potential of $S_3/S_2$ would have to be pH-dependent, concomitant with the $Y_Z^\bullet/Y_Z$ potential up to pH 7.9. Above pH 7.9, the $S_3/S_2$ redox couple would become pH-independent. When the pH is increased further to pH 8.5, the potentials of $S_3/S_2$ and $Y_Z^\bullet/Y_Z$ would be equal. However, we find this alternative

improbable. The argument originates from the pH titration curve in Figure 2 that fits reasonably well with a single deprotonation with only one proton leaving the OEC when the pH is increased. This also fits with the measured proton release in the $S_3$ state (*80*−*82*), and we have argued that this proton originates from $Y_Z$ and its hydrogen bond network. Therefore, it is likely that only one of the redox couples changes its potential at alkaline pH. This would rule out the first alternative with a pH-dependent $S_3/S_2$ potential which requires that one proton leaves $Y_Z$ and a second proton leaves the Mn cluster. Instead, we hypothesize that the $S_3/S_2$ couple is pH-independent in this interval and that the difference in redox potential between $S_3/S_2$ and $Y_Z^\bullet/Y_Z$ is larger than the 40 mV at pH 6 estimated by Vos (*79*, see also *15*) (Figure 8, dotted line).

Thus, we propose that only the potential of $Y_Z^\bullet/Y_Z$ is pH-dependent with the same pH dependence as observed in Tris-washed PSII (*83, 84*) and D1-His190 mutants lacking the Mn cluster (*28, 29*). To obtain a p*K* of 8.5 for the induction of the $S_2Y_Z^\bullet$ signal, the potential difference between the $S_3/S_2$ and $Y_Z^\bullet/Y_Z$ redox couples should be about 150 mV at pH 6−7, which gives a potential of about 820 mV for $S_3/S_2$ (Figure 8, dotted line). Another conclusion that can be drawn is that the p*K* of $Y_Z$ in intact PSII is at least 8.5 ± 0.3; otherwise, an observation of the $S_2Y_Z^\bullet$ signal would be impossible at pH 8.5.

It is probable that the $Y_Z^\bullet/Y_Z$ redox couple also can be affected by acidic pH. In this case, a change to pH 4 would increase the potential by 120 mV to ≈1100 mV. This is close to the potential of $P680^+$, and it is likely that the oxidation of $Y_Z$ would be dramatically slowed at lower pH values. In this case, recombination reactions between the acceptor side and $P680^+$ become more competitive and result in inhibition of the OEC. This is also observed, and steady-state oxygen evolution in PSII-enriched membranes is inhibited with a p*K* ≈ 4.7 (*15*). The mechanism for the low-pH inhibition of the oxygen evolution is not known. It has been implied that it reflects loss of $Ca^{2+}$ from its site in the OEC (*85*). In our experience, $Ca^{2+}$ is lost at lower pH values compared to where the oxygen evolution is blocked [see also Ono et al. (*62*)]. It is likely that the inhibition instead is due (at least partly) to the increased redox potential of $Y_Z$, making reduction of $P680^+$ inefficient.

There are several implications if the potential of the $Y_Z^\bullet/Y_Z$ redox couple changes as an effect of the changed pH value in the bulk solvent. $Y_Z$ is thought to be involved in a hydrogen-bonding network including His190 on the D1 protein (*3, 27*−*30*) and substrate water on the Mn cluster (*38, 61, 86*). If the redox potential of $Y_Z$ is sensitive to the ambient pH, this hydrogen-bonding network is likely to extend to the bulk solvent, at least in the $S_3$ state.

To our knowledge, this is the first direct evidence that $Y_Z$ is in direct contact with the bulk solvent in PSII with the Mn cluster present. This is a prerequisite for the H-atom abstraction mechanism which involves release of the phenolic proton of $Y_Z$ to the bulk solvent via the hydrogen-bonding network upon oxidation of $Y_Z$ in each S transition (*37, 87*). If the proton indeed can leave the $Y_Z$ environment when the pH is increased, as our data indicate, it should also be able to leave at physiological pH when $Y_Z$ becomes oxidized as has been proposed (*36*−*39*).

Figure 9 shows a proposal of the proton and electron movements upon oxidation of $S_2Y_Z$ to $S_3Y_Z$. First, $Y_Z^\bullet$ is

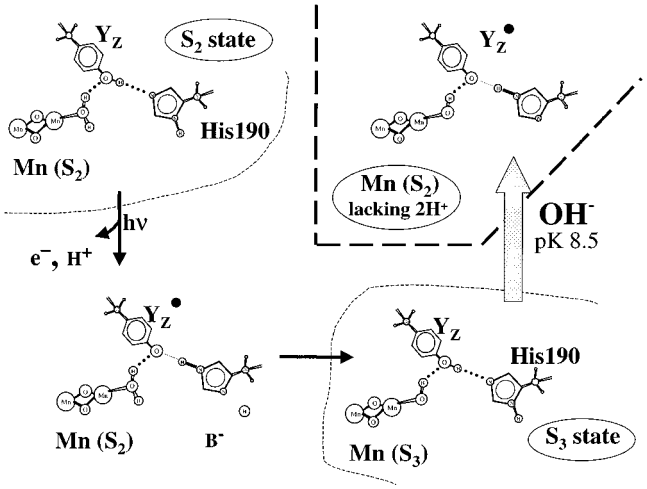


FIGURE 9: Electron transfer and deprotonation events involved in the $S_2 \rightarrow S_3$ transition and the pH-jump in the $S_3$ state. The upper left corner shows the imagined situation in the $Y_Z$-Mn moiety in the $S_2$ state. Only two of the manganese ions and one water molecule are shown. The phenolic oxygen is drawn hydrogen-bonded to His190 and also in contact with a water proton [compare schemes in (*37*−*39*)]. Upon oxidation of $Y_Z$, one electron leaves $P680^+$. At the same time, one proton leaves the system. It might leave either from $Y_Z$ (as drawn here) or from the water in the Mn cluster. In either case, the net result is the same, the $S_3$ state (lower right). Here the Mn cluster is in the $S_3$ valence configuration, and the $Y_Z$-Mn moiety is short one proton compared to the $S_2$ state. The reaction on the right shows what occurs when the pH is raised in the $S_3$ state. With a p*K* of 8.5, one proton leaves the system. We propose that the proton originates from the $Y_Z$-His190 hydrogen-bonding network. This lowers the redox potential of the $Y_Z^\bullet/Y_Z$ couple, causing $Y_Z$ to be oxidized by the Mn cluster, leading to the formation of $Y_Z^\bullet$ and the Mn cluster in the $S_2$ valence configuration. However, in this case the Mn−water system lacks two protons compared to the normal $S_2$ state. It should be pointed out that the model is independent of the exact molecular situation in $S_2$ with respect to protons and number and valence of the Mn atoms.

formed. As a consequence of this, the phenolic proton is found close to the nearby base (depicted as His190) or further away in the hydrogen-bonding network. Thereafter $Y_Z^\bullet$ is reduced by the Mn cluster. In this, or in the preceding step, one proton leaves the system. The proton leaves either from $Y_Z$-OH via His190 and the hydrogen-bonding network or from substrate water via another pathway.

In the first alternative, hydrogen-atom transfer to $Y_Z^\bullet$ catalyzes water oxidation, whereas the second alternative involves pure electron transfer from the Mn cluster to $Y_Z^\bullet$. In either case, the net result is that one electron and one proton have left the OEC (Figure 9). When base is added to the $S_3$ state, one more proton is removed from the system, this time from the $Y_Z$-His190 moiety as indicated by the p*K* for the reaction (Figure 9). This results in formation of the $S_2Y_Z^\bullet$ signal, and we can draw conclusions about the proton content in this system. The $S_2Y_Z^\bullet$ state originates from the $S_3$ state, which already is short of one proton compared to the $S_2$ state. However, we have removed one more proton by the addition of base. Thus, in our case, the $S_2Y_Z^\bullet$ redox state configuration lacks at least two protons that were present in the $S_2Y_Z$ state. One was removed in the normal flash-induced $S_2 \rightarrow S_3$ transition, and the second was removed by the alkaline pH treatment creating an abnormal proton deficiency around the $Y_Z$-His190 site.

This analysis might have relevance for the molecular events introduced in the OEC by $Ca^{2+}$-depletion. $Ca^{2+}$-

depletion has two effects on the donor side of PSII. First, it results in a perturbed form of the $S_2$ state which is very stable in the dark. The stability of the modified $S_2$ state most probably reflects a lowered redox potential compared to the normal $S_2$ state, making the modified $S_2$ state a less efficient substrate for recombination reactions (*45*). Second, $Y_Z^\bullet$ cannot drive the oxidation of the stable $S_2$ state, and the illumination gives rise to the $S_2Y_Z^\bullet$ radical instead (*45*).

A reasonable hypothesis is that the $S_2Y_Z^\bullet$ state has a similar origin in both $Ca^{2+}$-depleted PSII and alkaline pH-treated $S_3$ centers. In $Ca^{2+}$-depleted PSII, the $S_2$ state would then also be proton-deficient compared to the normal $S_2$ state. This conclusion is supported by the observation that the deprotonation that normally accompanies the $S_2 \rightarrow S_3$ transition is abolished in $Ca^{2+}$-depleted PSII (*71*). The proton deficiency would lower the redox potential of $S_2$, making it very stable. However, the lowered redox potential should also increase the driving force and thereby facilitate the oxidation of the modified $S_2$ by $Y_Z^\bullet$. This does not occur, and instead the oxidation is completely blocked. Therefore, other arguments must be invoked to explain the inability of $Y_Z^\bullet$ to oxidize the Mn cluster. We propose that the reason is the mechanism for the reduction of $Y_Z^\bullet$.

The main feature in the hydrogen-atom transfer mechanism for water oxidation (*36*−*39*, *87*) is that the tyrosine radical needs both an electron and a proton from the Mn cluster. We argue that there is no proton available in the Mn cluster in the $Ca^{2+}$-depleted $S_2$ state and that the block induced by $Ca^{2+}$-depletion therefore is due to the inability of the Mn cluster to provide both an electron and a proton to $Y_Z^\bullet$. This argument supports an earlier proposal that $Ca^{2+}$ regulates the deprotonation associated with the water oxidation (*88*).

We can also draw conclusions about the pH dependence of the redox potential in the $S_2$ state. The oxidizing potential of $S_2$ is thought to be very similar to that of $S_3$ (*15*). However, the increased pH, which decreases the potential of $Y_Z^\bullet$ in $S_3$, does not seem to induce a tyrosine-derived radical when the same pH-jump experiment is performed in $S_2$ (*58*). There are two possible reasons for this: either the group that titrates is completely different in $S_2$ and $S_3$ or the titration affects the redox potential of $S_2$ in parallel to the potential of $Y_Z$.

In our earlier study (*58*), the pH effect on the multiline EPR signals in $S_0$ and $S_2$ was investigated. The p*K* values for the disappearance of the multiline signals, 8.0 in $S_0$ and 7.6 in $S_2$, were quite similar, and it was suggested that the same group was involved (*58*). These p*K* values are not too different from the p*K* observed in this study of $S_3$ (p$K$ = 8.5). Therefore, we propose that the titration at alkaline pH affects the hydrogen-bonding network around $Y_Z$ in all S states in a similar way. If this hypothesis is correct, a likely explanation for why $Y_Z^\bullet$ is not induced at high pH in $S_2$ is that also the redox potential of $S_2$ is pH-dependent as indicated in Figure 7. This is feasible, as the Mn cluster in the $S_2$ state is proton-rich compared to $S_3$ (Figure 9).

## CONCLUSIONS

The spin-coupled EPR signal proposed to arise from the $S_2Y_Z^\bullet$ state can be formed by titration of PSII at alkaline pH in the dark in the $S_3$ state. The formation of the signal by changes in the ambient pH indicates that the phenolic proton of $Y_Z$ is titrated. The access to the bulk solvent is proposed to be via a hydrogen-bonding network, and this can be titrated in all S states. The sensitivity of the hydrogen-bonding network to the ambient pH also means that protons can be released efficiently via this pathway as $Y_Z$ is oxidized. This lowers the p*K* of the phenolic proton of $Y_Z$ to very low values (*37*, *87*). The deprotonation of $Y_Z$ is a crucial step in the H-atom abstraction mechanism for water oxidation, and we consider our experiments to be in favor of this mechanism, at least in the $S_2 \rightarrow S_3$ transition. This also holds for the comparison with $Ca^{2+}$-depleted PSII, which are proposed to be inhibited between $S_2$ and $S_3$ due to a lack of protons in the OEC in the $S_2$ state. The proton must accompany the electron in the reduction of $Y_Z^\bullet$, again arguing for the vital coupling of electron and proton transfer between the Mn cluster and $Y_Z$.

## ACKNOWLEDGMENT

We appreciate valuable discussions and advice about the $Ca^{2+}$-depletion procedure from Drs. Warwick Hillier and Yashar Feyziev. We also thank Dr. Yashar Feyziev for invaluable help with the $Ca^{2+}$-depletion preparation and Dr. Bart van Rotterdam for advice on the kinetic considerations. Drs. Fikret Mamedov and Gerald Babcock are also acknowledged for their useful comments on the manuscript.

## REFERENCES

1. Barber, J., Nield, J., Morris, E. P., Zheleva, D., and Hankamer, B. (1997) *Physiol. Plant. 100*, 817−827.
2. Debus, R. J. (2000) in *Manganese and Its Role in Biological Processes* (Sigel, A., and Sigel, H., Eds.) pp 657−710, Marcel Dekker, Inc., Basel, Switzerland.
3. Svensson, B., Etchebest, C., Tuffery, P., van Kan, P. J. M., Smith, J., and Styring, S. (1996) *Biochemistry 35*, 14486−14502.
4. Rhee, K. H., Morris, E. P., Barber, J., and Kühlbrandt, W. (1998) *Nature 396*, 282−286.
5. Diner, B. A., and Babcock, G. T. (1996) in *Oxygenic Photosynthesis: The Light Reactions* (Ort, D. R., and Yocum, C. F., Eds.) pp 213−247, Kluwer Academic Press, Dordrecht, The Netherlands.
6. Renger, G. (1997) *Physiol. Plant. 100*, 828−841.
7. Debus, R. J. (1992) *Biochim. Biophys. Acta 1102*, 269−352.
8. Yachandra, V. K., Sauer, K., and Klein, M. P. (1996) *Chem. Rev. 96*, 2927−2950.
9. Åhrling, K. A., Peterson, S., and Styring, S. (1997) *Biochemistry 36*, 13148−13152.
10. Messinger, J., Robblee, J. H., Yu, W. O., Sauer, K., Yachandra, V. K., and Klein, M. P. (1997) *J. Am. Chem. Soc. 119*, 11349−11350.
11. Dau, H., Iuzzolino, L., and Dittmer, J. (2001) *Biochim. Biophys. Acta 1503*, 24−39.
12. Kuzek, D., and Pace, R. J. (2000) *Biochim. Biophys. Acta 1503*, 123−137.
13. Pecoraro, V. L., and Hsieh, W.-Y. (2000) in *Manganese and Its Role in Biological Processes* (Sigel, A., and Sigel, H., Eds.) pp 429−504, Marcel-Dekker, Inc., Basel, Switzerland.
14. Kok, B., Forbush, B., and McGloin, M. (1970) *Photochem. Photobiol. 11*, 457−475.
15. Vass, I., and Styring, S. (1991) *Biochemistry 30*, 830−839.
16. Britt, D. R. (1996) in *Oxygenic Photosynthesis: The Light Reactions* (Ort, D. R., and Yocum, C. F., Eds.) pp 137−164, Kluwer Academic Publishers, Dordrecht, The Netherlands.
17. Iuzzolino, L., Dittmer, J., Dörner, W., Meyer-Klaucke, W., and Dau, H. (1998) *Biochemistry 37*, 17112−17119.
18. Yachandra, V. K., DeRose, V. J., Latimer, M. J., Mukerji, I., Klein, M. P., and Sauer, K. (1993) *Science 260*, 675−679.
19. Hillier, W., and Wydrzynski, T. (2000) *Biochemistry 39*, 4399−4405.
20. Hillier, W., and Wydrzynski, T. (2000) *Biochim. Biophys. Acta 1503*, 197−209.

21. Styring, S., and Rutherford, A. W. (1988) *Biochemistry 27*, 4915−4923.
22. Evelo, R. G., Styring, S., Rutherford, A. W., and Hoff, A. J. (1989) *Biochim. Biophys. Acta 973*, 428−442.
23. Liang, W., Roelofs, T. A., Cinco, R. M., Rompel, A., Latimer, M. J., Yu, W. O., Sauer, K., Klein, M. P., and Yachandra, V. K. (2000) *J. Am. Chem. Soc. 122*, 3399−3412.
24. Srinivasan, A. N., and Sharp, R. R. (1986) *Biochim. Biophys. Acta 851*, 369−376.
25. Ono, T., Noguchi, T., Inoue, Y., Kusunoki, M., Matsushita, T., and Oyanagi, H. (1992) *Science 258*, 1335−1337.
26. Special issue "Photosynthetic water oxidation" (Nugent, J., Ed.) (2001) *Biochim. Biophys. Acta 1503*, (1).
27. Svensson, B., Vass, I., Cedergren, E., and Styring, S. (1990) *EMBO J. 9*, 2051−2059.
28. Mamedov, F., Sayre, R. T., and Styring, S. (1998) *Biochemistry 37*, 14245−14256.
29. Hays, A.-M. A., Vassiliev, I. R., Golbeck, J. H., and Debus, R. J. (1998) *Biochemistry 37*, 11352−11365.
30. Hays, A.-M. A., Vassiliev, I. R., Golbeck, J. H., and Debus, R. J. (1999) *Biochemistry 38*, 11851−11865.
31. Ahlbrink, R., Haumann, M., Cherepanov, D., Bögerhausen, O., Mulkidjanian, A., and Junge, W. (1998) *Biochemistry 37*, 1131−1142.
32. Haumann, M., and Junge, W. (1999) *Biochim. Biophys. Acta 1411*, 86−91.
33. Rappaport, F., Blanchard-Desce, M., and Lavergne, J. (1994) *Biochim. Biophys. Acta 1184*, 178−192.
34. Haumann, M., Bögerhausen, O., Cherepanov, D., Ahlbrink, R., and Junge, W. (1997) *Photosynth. Res. 51*, 192−208.
35. Karge, M., Irrgang, K.-D., and Renger, G. (1997) *Biochemistry 36*, 8904−8913.
36. Hoganson, W. C., Lydakis-Simantiris, N., Tang, X.-S., Tommos, C., Warncke, K., Babcock, G. T., Diner, B. A., McCracken, J., and Styring, S. (1995) *Photosynth. Res. 46*, 177−184.
37. Tommos, C., and Babcock, G. T. (2000) *Biochim. Biophys. Acta 1458*, 199−219.
38. Hoganson, W. C., and Babcock, G. T. (1997) *Science 277*, 1953−1956.
39. Tommos, C., and Babcock, G. T. (1998) *Acc. Chem. Res. 31*, 18−25.
40. Metz, J. G., Nixon, P. J., Rögner, M., Brudvig, G. W., and Diner, B. A. (1989) *Biochemistry 28*, 6960−6969.
41. Westphal, K. L., Tommos, C., Cukier, R. I., and Babcock, G. T. (2000) *Curr. Opin. Plant Biol. 3*, 236−242.
42. Blomberg, M. R. A., Siegbahn, P. E. M., Styring, S., Babcock, G. T., Åkermark, B., and Korall, P. (1997) *J. Am. Chem. Soc. 119*, 8285−8292.
43. Matsukawa, T., Mino, H., and Kawamori, A. (1999) *Biochemistry 38*, 4072−4077.
44. Ioannidis, N., and Petrouleas, V. (2000) *Biochemistry 39*, 5246−5254.
45. Boussac, A., Zimmermann, J.-L., and Rutherford, A. W. (1989) *Biochemistry 28*, 8984−8989.
46. Sivaraja, M., Tso, J., and Dismukes, G. C. (1989) *Biochemistry 28*, 9459−9464.
47. Ono, T., and Inoue, Y. (1989) *Biochim. Biophys. Acta 973*, 443−449.
48. Gilchrist, M. L., Ball, J. A., Randall, D. W., and Britt, R. D. (1995) *Proc. Natl. Acad. Sci. U.S.A. 92*, 9545−9549.
49. MacLachlan, D. J., and Nugent, J. H. A. (1993) *Biochemistry 32*, 9772−9780.
50. Szalai, V. A., and Brudvig, G. W. (1996) *Biochemistry 35*, 1946−1953.
51. Force, D. A., Randall, D. W., and Britt, R. D. (1997) *Biochemistry 36*, 12062−12070.
52. Dorlet, P., Di Valentin, M., Babcock, G. T., and McCracken, J. L. (1998) *J. Phys. Chem. B 102*, 8239−8247.
53. Dorlet, P., Boussac, A., Rutherford, A. W., and Un, S. (1999) *J. Phys. Chem. B 103*, 10945−10954.
54. Lakshmi, K. V., Eaton, S. S., Eaton, G. R., Frank, H. A., and Brudvig, G. W. (1998) *J. Phys. Chem. B 102*, 8327−8335.
55. Pace, R. J., Smith, P., Bramley, R., and Stehlik, D. (1991) *Biochim. Biophys. Acta 1058*, 161−170.
56. Arnon, D. I. (1949) *Plant Physiol. 24*, 1−15.
57. Styring, S., and Rutherford, A. W. (1987) *Biochemistry 26*, 2401−2405.
58. Geijer, P., Deák, Z., and Styring, S. (2000) *Biochemistry 39*, 6763−6772.
59. Ono, T., and Inoue, Y. (1988) *FEBS Lett. 227*, 147−152.
60. Andréasson, L.-E., Vass, I., and Styring, S. (1995) *Biochim. Biophys. Acta 1230*, 155−164.
61. Tommos, C., McCracken, J., Styring, S., and Babcock, G. T. (1998) *J. Am. Chem. Soc. 120*, 10441−10452.
62. Ono, T., and Inoue, Y. (1990) *Biochim. Biophys. Acta 1015*, 373−377.
63. Dismukes, G. C., and Siderer, Y. (1981) *Proc. Natl. Acad. Sci. U.S.A. 78*, 274−278.
64. Boussac, A., and Rutherford, A. W. (1990) *FEBS Lett. 277*, 69−74.
65. Lydakis-Simantiris, N., Dorlet, P., Ghanotakis, D. F., and Babcock, G. T. (1998) *Biochemistry 37*, 6427−6425.
66. Boussac, A. (1996) *Biochim. Biophys. Acta 1277*, 253−265.
67. Boussac, A., Sétif, P., and Rutherford, A. W. (1992) *Biochemistry 31*, 1224−1234.
68. MacLachlan, D. J., Nugent, J. H. A., Warden, J. T., and Evans, M. C. W. (1994) *Biochim. Biophys. Acta 1188*, 325−334.
69. Szalai, V. A., Kühne, H., Lakshmi, K. V., and Brudvig, G. W. (1998) *Biochemistry 37*, 13594−13603.
70. Boussac, A., and Rutherford, A. W. (1992) *Biochemistry 31*, 7441−7445.
71. Boussac, A., Zimmermann, J.-L., Rutherford, A. W., and Lavergne, J. (1990) *Nature 347*, 303−306.
72. Ono, T., and Inoue, Y. (1990) *Biochim. Biophys. Acta 1020*, 269−277.
73. Baumgarten, M., Philo, J. S., and Dismukes, G. C. (1990) *Biochemistry 29*, 10814−10822.
74. Peloquin, J. M., Campbell, K. A., and Britt, R. D. (1998) *J. Am. Chem. Soc. 120*, 6840−6841.
75. Babcock, G. T., Blankenship, R. E., and Sauer, K. (1976) *FEBS Lett. 61*, 286−289.
76. Razeghifard, M. R., and Pace, R. J. (1997) *Biochim. Biophys. Acta 1322*, 141−150.
77. Razeghifard, M. R., and Pace, R. J. (1999) *Biochemistry 38*, 1252−1257.
78. Tommos, C., Skalicky, J. J., Pilloud, D. L., Wand, A. J., and Dutton, P. L. (1999) *Biochemistry 38*, 9495−9507.
79. Vos, M. H. (1990) Ph.D. Thesis, University of Leiden, Leiden, The Netherlands.
80. Rappaport, F., and Lavergne, J. (1991) *Biochemistry 30*, 10004−10012.
81. Schlodder, E., and Witt, H. T. (1999) *J. Biol. Chem. 274*, 30387−30392.
82. Lavergne, J., and Junge, W. (1993) *Photosynth. Res. 38*, 279−296.
83. Yerkes, C. T., Babcock, G. T., and Crofts, A. R. (1983) *FEBS Lett. 158*, 359−363.
84. Conjeaud, H., and Mathis, P. (1986) *Biophys. J. 49*, 1215−1221
85. Krieger, A., Weis, E., and Demeter, S. (1993) *Biochim. Biophys. Acta 1144*, 411−418.
86. Noguchi, T., Inoue, Y., and Tang, X.-S. (1997) *Biochemistry 36*, 14705−14711.
87. Tommos, C., Tang, X.-S., Warncke, K., Hoganson, W. C., Styring, S., McCracken, J., Diner, B. A., and Babcock, G. T. (1995) *J. Am. Chem. Soc. 117*, 10325−10335.
88. Rutherford, A. W., Zimmermann, J.-L., and Boussac, A. (1992) in *The Photosystems: Structure, Function and Molecular Biology* (Barber, J., Ed.) pp 179−229, Elsevier Science Publishers B. V, Amsterdam, The Netherlands.
89. Thorp, H. H., Sarneski, J. E., Brudvig, G. W., and Crabtree, R. H. (1989) *J. Am. Chem. Soc. 111*, 9249−9250.
90. Baldwin, M. J., Gelasco, A., and Pecoraro, V. L. (1993) *Photosynth. Res. 38*, 303−308.


BI010040V